HHS Public Access

Author manuscript

Angew Chem Int Ed Engl. Author manuscript; available in PMC 2016 February 16.

Published in final edited form as:

Angew Chem Int Ed Engl. 2015 February 16; 54(8): 2525–2529. doi:10.1002/anie.201410754.

Tunable Release of Multiplex Biochemicals by Plasmonic-Active Rotary Nanomotors

Xiaobin Xu[a],[b], **Kwanoh Kim**[b], and **Prof. Dr. D. L. Fan**[a],[b]

D. L. Fan: dfan@austin.utexas.edu

[a]Materials Science and Engineering Program, Texas Matrials Insititute, The University of Texas at Austin, Austin, Austin, TX 78712, USA

[b]Mechanical Engineering, The University of Texas at Austin, Austin, Austin, TX 78712, USA

Abstract

It is highly desirable to precisely tune the molecule release rate from the surfaces of nanoparticles (NPs), relevant to cancer therapy and single-cell biology. Here, we report an innovative mechanism to actively tune the biochemical release rate by rotation of NPs. Plasmonic nanomotors were assembled from NPs and applied in multiplex biochemical release and detection. Both single and multiplex biosignals can be released in a tunable fashion by controlling the rotation speed of the nanomotors. The chemistry and release rate of individual chemicals can be revealed by Raman spectroscopy. The fundamental mechanism was modeled quantitatively and attributed to the fluidic boundary-layer reduction due to the liquid convection. This work, which explored the synergistic attributes of surface enhanced Raman scattering and nanoelectromechanical systems, could inspire a new sensor scheme, potentially interesting for various bio-applications.

Keywords

nanomotors; SERS; biosensing; drug release; nanorobotics

The great potentials of nanoparticles for biosubstance delivery have intrigued considerable research interest owing to their controllable geometry, chemistry, and surface functionality[1]. Various nanoentities were explored for in-vivo drug delivery and cancer therapy[1],[2]. Among them, one-dimensional nanoentities, such as nanowires and nanotubes, received special attentions, whose lengths and diameters could be controlled to the scales of live cells and biomolecules, respectively[3]. They were applied as vehicles for transporting biospecies, such as cytokines[4], peptide[5], enzymes[6], and genes[7], for in-vitro stimulation[4]. Nevertheless, it remains a grand challenge to release biosubstances attached on nanoparticles in a tunable fashion, the feast of which could enable an in-depth understanding of the fundamental sciences in drug delivery, single cell stimulation, and cell-cell communications[4].

Correspondence to: D. L. Fan, dfan@austin.utexas.edu.

Supporting information for this article is given via a link at the end of the document.

Previously, pulsed electric potentials were employed to release biosubstances from patterned microelectrodes[8], demonstrating the feasibility of electric-induced biochemical release from nanoparticles. However, this intriguing mechanism requires complex lithographical patterning to electrically connect nanoparticles. Recently, heat generated from optical excitation of plasmonic nanoparticles was used for releasing gene molecules[9]. Vibrations induced by the radio-frequency electromagnetic fields were also used to enhance the releasing rate of drug molecules[10]. Recently, self-propelled nanomotors were used to active release desired ions.[11] Acoustic-driven nanomotors were acturated inside live cells[12]. Nevertheless, it remains a daunting task to tune the molecular release rate from individual nanoparticles with high precision while monitoring it simultaneously.

Recently, we reported an innovative type of electric-driven nanomotors assembled from nanoscale building blocks with ultrahigh speed and fixed rotation positions. Preliminary study demonstrates the controlled release of biochemicals from such nanomotors[13]. However, systematic study has not been conducted, which is highly desirable to understand the fundamental mechanism. It is also of great interest to release more than one type of molecules from the nanomotors.

In this research, we systematically investigated the concept of motorization of plasmonic nanosensors for tuning the release rate of biochemicals, their real-time detection, and the underline mechanism via experimentation and analytical modeling. The nanomotors, with enhanced functionalities in both molecular sensing and actuation, were assembled from designed plasmonic nanoparticles and patterned nanomagnets, and rotated with controlled speed and chirality by the electric tweezers [14]. Both single and multiple analytes can be released in a tunable fashion by the mechanical rotation of the nanomotors. The chemistry and concentration of individual analytes were revealed simultaneously by using high-speed micro-Raman spectroscopy. The fundamental mechanism was investigated and attributed to the convection induced fluidic boundary-layer reduction, which quantitatively agrees with the experimental results. To the best of our knowledge, this effect is observed and unerstood in the micro/nanomechanical system for the first time. This research, exploring robotized nanomotor sensors by integrating SERS[15] and NEMS, could be of interest for bio-relevant applications [4, 12, 16]

The designed the nanomotor system consist of plasmonic-sensitive nanorod as rotors, patterned nanomagnets as bearings, and microelectrodes as stators as shown in Fig. 1a. The plasmonic naonrotor, the most critical component of a nanomotor for attaching and detecting biochemicals, has a tri-layer structure with a core made of a Au/Ni/Au three-segment nanowire, a layer of silica conformably coated on the nanowire core, and uniformly surface-distributed Ag nanoparticles (NPs) synthesized on the outer surface of silica [Fig. 1a]. Here, each layer of the plasmonic nanorotor was designed to serve for a purpose: the metallic nanowire core can be efficiently polarized in electric fields for fast transport and rotation by our recent invention— the electric tweezers[14]; the Ni-segment presented in the nanowire core assists the anchorage of the plasmonic nanorotor on a pre-patterned nanomagnet into a nanomotor[13]; and the mesoporous silica coating with densely surface-distributed Ag NPs (~1570/μm^2) provides efficient absorption of molecules and their ultrasensitive Raman detection[17]. It is worth noting that it shows that Ag NPs are biocompatibility when their

concentration is below a certain thresh-hold, suggesting a window for the bio-application of Ag NPs[18]. Au NPs could be more advantageous in terms of a higher biocompatibility, while the Raman enhancement effect of which is generally lower than that of Ag NPs in the visiable regime[19].

Three steps were taken to fabricate the plasmonic rotors. In brief, the multi-segment Au/Ni/Au nanowires (300 nm in diameter) were synthesized by electrodeposition into nanoporous templates[14a, 20]. before a 70-nm-thick silica layer being conformably coated on the outer surface of nanowires via the hydrolysis of tetraethyl orthosilicate[21]. Next, a large array of Ag NPs were synthesized uniformly on the surface of silica in a mixture of silver nitrite and ammonia via catalysis of polyvinylpyrrolidone (PVP) for 7 hours at 70°C[21]. Finally, the as-synthesized nanowire rotors were sonicated, centrifuged and washed before redispersed in deionized (D.I.) water. The experimental details were provided in the supporting information.

Scanning electron microscopy (SEM) confirmed the successful synthesis of the tri-layered plasmonic rotors as shown in Figs. 1b–c. The Ag NPs, densely distributed on the rotor surfaces, were semi-spherical with an average diameter of ~25.2±6.4 nm and density of ~1570/μm^2. If considering the NP junctions of less than 2 nm as the plasmonic hotspots, where Raman signals of molecules can be substantially enhanced due to ultrahigh electric fields generated by the coherence oscillation of conduction-band electrons[22], we found the density of hotspots can be as high as ~1300/μm^2. These hotspots distributed along the plasmonic nanorotor essentially uniformly as shown in the Raman mapping of Rhodamine-6G (R6G) molecules (Fig. 1d, 1 μM R6G incubated with the plasmonic nanorotor for 2 hrs before dried). Here, the Raman image was taken from a single plasmonic nanorotor by using a confocal Raman microscope exciting at 532 nm with a step size of 250 nm and a spot size of ~1 μm. The integration time of each spectrum was set at 0.5 second. The Raman enhancement factor of such kind of plasmonic nanorotors can be estimated as ~10^{10} following a method reported previously [23], one of the highest among the state-of-the-art[24]. In the control experiment, we did SERS characterization of NB (340 nM) from a nanorod without Ag NPs, i.e. silica coated Au-Ni-Au nanorod. No NB signal can be detected. (See Fig. S2)

The strong Raman enhancement and high density of hotspots on the plasmonic nanorotors are pivotal for ultrasensitive SERS detection.[15b, 15c] Using them, we can readily determine both the chemistry and concentration of multiple molecules simultaneously with Raman spectroscopy. Nile blue (NB) and R6G, two commonly used SERS probes, were employed for the demonstration purpose due to their large Raman scattering cross-sections and wide biological applications[25]. A series of R6G and NB in D.I. water suspension were incubated with the plasmonic nanorotors for 30 min. Then the Raman spectra were collected by using a Raman microscope equipped with 532 and 632.8 nm lasers. It was shown that the Raman intensity monotonically increased with the concentration of NB (or R6G), from which, one can quantitatively determine the concentrations of analytes (Fig. S1a–e). Note that we measured multiple plasmonic nanorotors deposited on the substrate to obtain the average of Raman intensity for each concentration. The detection is highly sensitive that the time-

dependent absorption of biomolecules (NB, 50 nM) to their surfaces can be monitored, which shows a monotonic increase before reaching a saturation plateau at ~70 sec (Fig. S1f).

More importantly, the structure of the plasmonic nanorotor was carefully designed for robotization. The nanomotors consist of the plasmonic rotors serving as nanomotor rotors and patterned nanomagnets as bearings (a thin film stack of Au (100 nm)/Ni (80 nm)/Cr (6 nm), 1 μm in diameter) (Fig. 1a). To assemble such nanomotors, we employed the electric tweezers— a recently developed nanomanipulation technique that can align and transport nonspherical nanoentities with a precision of at least 300 nm [14a, 26]. The randomly suspended plasmonic nanorotors were manipulated in both the X and Y directions. The transport velocity increased linearly with the applied DC voltages (Fig. 2a). When the plasmonic nanorotors were in the vicinity of the nanomagnets, they were swiftly attracted and assembled on the nanomagnets due to the magnetic attraction. Then, a rotating electric field was generated by four AC electric voltages with sequential 90° phase-shift applied to the quadruple microelectrodes, which compelled the assembled nanomotors into rotation (Fig. 1a, Figs. 2b, Video S1).

The rotation is a result of the induced electric torque (T_e) generated from the interactions between the polarized plasmonic nanorotors and the external AC electric field[14b, 27], where $T_e \sim E^2$. The E^2 dependence of the rotation speed (ω) counts for its V^2 dependence in Fig. 2c. In addition to the applied voltage, the speed of the nanomotor sensors can also be optimized by the applied AC frequency, where the highest value obtained at 50 kHz in the range of 10 to 100 kHz (Fig. 2d). As a result, the nanomotor sensors can be successfully synthesized, assembled, and actuated with high sensitivity for biochemical detection and controllability in mechanical rotation.

Next, we investigated the applications of nanomotors for tuning the biochemical release and the involved fundamental mechanisms. Both the releases of single (NB) and multiplex biochemicals (mixture of NB and R6G) were studied. The molecules were functionalized on the surface of the plasmonic nanorotors by incubation followed by redispersion in D.I. water [supporting information]. Immediately after the dispersion, the plasmonic nanorotors were quickly assembled into nanomotors and rotated (Video S1). The distribution of molecules on the surface of nanomotors can also be directly imaged and videotaped detected by the ultrasensitive high-speed CCD camera at a frame rate of 24 f/s from their Raman images (Fig. 2e and Video S2). In the study of molecule release of NB, the rotation speed of nanomotors was precisely controlled from 195 rpm to 75 rpm at 17 to 10 V (Video S3). The molecule release rate from the surface of the rotating nanomotor was monitored and recorded simultaneously by using a high-speed Raman spectroscopy operating at 0.5 spectrum/s (Figs. 3a–b). The release of molecules (340 nM NB) from the surface of a rotating nanomotor (126 rpm) can be detected for a long duration, e.g. 30 min, as shown Fig. S4. The molecule release from a static nanomotor is also shown in Fig. S5.

It was found that, regardless of the rotation speed or the molecular species, the concentration of molecules measured with the Raman spectroscopy decreases with time monotonically. Note that only those molecules attached on the surface of the nanomotor sensors can be detected, due to the significant plasmonic enhancement from the Ag NPs. Also the

molecular concentration on the surface of nanomotors was much higher than that in the bulk solution. As a result, a net molecular mass flow can be established from the nanomotor sensors to the bulk solution, consistent with the monotonic concentration decrease as observed in the Raman spectroscopy.

This phenomenon can be modeled by using the Nernst diffusion-layer theory, which is widely used to understand phenomena involving solid-liquid interfaces[28]. According to this theory, at the interface of a solid surface and a suspension medium, a stationary liquid layer is formed with a thickness of λ. Within such a stationary layer, the transport of mass between the solid surface and bulk liquid, such as molecules or ions, can only occur by the passive diffusion in the direction of the chemical gradient. Out of such a region, liquid convection dominates, which can actively pump molecules to the outer boundary of the stationary layer. If the concentration of the analyte molecules at the layer boundary is approximated to be the same as that in the bulk solution, a static concentration gradient can be established across this stationary diffusion layer as shown in Fig. 5. According to the Fick's diffusion laws, the time dependence concentration of molecules on the surface of nanomotors (C) can be calculated as:

$$C = C' \cdot e^{-kt} + C_0 \quad (1)$$

where $C' = C_1 - C_0$, C_1 is the initial concentrations of NB on the surface of nanomotors, C_0 is the concentration of NB in the bulk solution, and k (unit of 1/second) is the molecule release rate. The value of k is proportional to D/λ, where D is the diffusion coefficient of the NB molecules. From Eq. (1), we can readily determine the rate of molecule release when the nanomotor sensors were rotated at different speeds (ω). Here, at each rotation speed, the data points was fitted according to Eq. (1) by using Origin software with the initial C_1 given as the as-measured values (Fig. 3a–b). Interestingly, the molecule release rate (k) monotonically increased with the rotation speed with a power-law dependence of $k \sim \omega^{0.51}$ (Fig. 3c). It is highly direable to understand the governing mechanism of such a relation. We attribute the mechanism to the stationary diffusion layer reduction as a result of the liquid convection due to the rotation of nanomotors. According to the classical boundary layer theory[33], a flow with a speed of v passing on a flat surface can result in the thinning of the stationary layer next to the solid surface due to fluidic convection promoted by the flow, whereas the thickness of the stationary layer follows the relation of $\lambda \sim R_e^{-0.5} \sim \nu^{-0.5}$ [29]. Given the molecular release rate of $k \sim D/\lambda \sim 1/\lambda$ and the fluidic velocity (v) proportional to the rotation speed (ω) of nanomotor sensors ($v \sim \omega$), it can be readily known that $k \sim \sqrt{\omega}$, which quantitatively agrees with our experimental observation of $k \sim \omega^{0.51}$ (Fig. 3c). Moreover, we note that the theory for the rotating disk electrode (RDE) system, studied extensively in electrochemistry[28], further supports our understanding, which indicates that the transport of ionic masses to a rotating disk electrode increases with the rotation speed of the electrode with a power-law dependence of 0.5 [28, 30].

It is also important to know whether the applied AC electric (E) fields could directly alter the molecule release rate[27b]. A control experiment was performed on a stationary nanomotor functionalized with NB molecules. The AC rotating E-fields (17 V, 20 kHz) were turned on and off alternately for multiple times, while the molecular release was

monitored simultaneously. The molecular release rate remained unchanged when the *E*-field was either on or off, which suggests that the AC *E*-field has negligible effect on molecule release rate (Fig. S3). This experiment was repeated many times to confirm the observation.

The next question is whether the above mechanism is applicable to the release of multiplex biochemicals. To address this question, we functionalized the nanomotor sensors with a mixture of NB and R6G, rotated them from 240 to 130 rpm at 18 to 14 V, 50 kHz, and collected the time-dependent Raman signals of both analytes. Since each type of molecule has its unique Raman spectrum, the chemistry as well as the concentration of each analyte on the surface of nanomotors can be determined simultaneously (Fig. 4a–c). By employing the same fitting method used for the single chemical release, we determined the release rate (k) of each biochemical at different rotation speed (ω). Both showed linear increment with ω with a power-law dependence of 0.52 and 0.53 for NB and R6G, respectively (Fig. 4d). The results demonstrated that the release of multiplex biochemicals has the dependence of $k \sim \omega^{0.51}$, same as that of single analyte release, which suggests that the aforediscussed model used for single moelcule release can be applied to understand the multiplex release. Moreover, we note that the release rate of NB (k: 0.0076 ~ 0.0123 s^{-1}) in the multiplex release system is consistently higher than that obtained as a single analyte (k: 0.0017~0.0044 s^{-1}). This could be attributed to the higher concentration and release rate of R6G molecules in the multiplex sample, where the dominating R6G could assist the detachment of NB molecules from the nanomotor sensors during its release and thus increased the release rate of NB. Here, a much higher concentration of R6G is necessary in the mixed sample (R6G:~20 μM, NB:~ a few nM) in order to obtain signals from both molecules on a similar level, which could be due to the much poorer attachment of R6G to Ag NPs than that of NB.

In summary, we investigated a new mechanism for tuning the release rate of biochemicals from the surface of nanoparticles via controlled mechanical rotation. The investigation was carried out by both experimentation and analytic modeling. We synthesized, assembled and rotated plasmonic nanomotors for this study. The kinetics of molecules release from the nanomotors was monitored by high-speed Raman spectroscopy. Both single and multiple analytes can be released at desirable rates by controlling the rotation speeds of nanomotors. The release rate shows a power-law dependence of approximately 0.5 with the rotation speed. The fundamental mechanism can be attributed to the convection-induced thickness reduction of the diffusion layer, which agrees with the experimental results quantitatively. To our best knowledge, such an effect is observed on micro/nanoscale devices for the first time. The nanomotor sensors could be potentially interesting for various bio-relevant applications, such as tunable biochemical release in an in-vitro setting, although great efforts should be spent to work out the technical details and demonstrations. This research could potentially inspire a new device scheme of robotized SERS sensors.

Supplementary Material

Refer to Web version on PubMed Central for supplementary material.

Acknowledgments

We are grateful for the support of National Institute of Health (NIH) (Grant No. 9R42ES024023-02), Welch Foundation (Grant No. F-1734), NSF (Career Award CMMI-1150767 and ECCS-1446489), and Research Grant from the Office of Vice President for Research, University of Texas at Austin.

References

1. Doane TL, Burda C. Chem Soc Rev. 2012; 41:2885. [PubMed: 22286540]
2. a) Bardhan R, Chen W, Bartels M, Perez-Torres C, Botero MF, McAninch RW, Contreras A, Schiff R, Pautler RG, Halas NJ, Joshi A. Nano Lett. 2010; 10:4920–4928. [PubMed: 21090693] b) Choi MR, Stanton-Maxey KJ, Stanley JK, Levin CS, Bardhan R, Akin D, Badve S, Sturgis J, Robinson JP, Bashir R, Halas NJ, Clare SE. Nano Lett. 2007; 7:3759–3765. [PubMed: 17979310]
3. Xu X, Li H, Hasan D, Ruoff RS, Wang AX, Fan DL. Adv Funct Mater. 2013; 23:4332–4338.
4. Fan D, Yin Z, Cheong R, Zhu FQ, Cammarata RC, Chien CL, Levchenko A. Nature Nanotech. 2010; 5:545–551.
5. Xu ZP, Zeng QH, Lu GQ, Yu AB. Chem Eng Sci. 2006; 61:1027–1040.
6. Orozco J, Vilela D, Valdés-Ramírez G, Fedorak Y, Escarpa A, Vazquez-Duhalt R, Wang J. Chemistry - A European Journal. 2014; 20:2866–2871.
7. Salem AK, Searson PC, Leong KW. Nature Materials. 2003; 2:668–671.
8. a) Wildt B, Wirtz D, Searson PC. Nature Protocols. 2010; 5:1273–1280.b) Mali P, Bhattacharjee N, Searson PC. Nano Lett. 2006; 6:1250–1253. [PubMed: 16771589]
9. Lee SE, Liu GL, Kim F, Lee LP. Nano Lett. 2009; 9:562–570. [PubMed: 19128006]
10. Peiris PM, Bauer L, Toy R, Tran E, Pansky J, Doolittle E, Schmidt E, Hayden E, Mayer A, Keri RA, Griswold MA, Karathanasis E. ACS Nano. 2012; 6:4157–4168. [PubMed: 22486623]
11. Soler L, Magdanz V, Fomin VM, Sanchez S, Schmidt OG. ACS Nano. 2013; 7:9611–9620. [PubMed: 24180623]
12. Wang W, Li S, Mair L, Ahmed S, Huang TJ, Mallouk TE. Angew Chem. 2014; 126:3265–3268.
13. Kim K, Xu X, Guo J, Fan DL. Nat Commun. 2014; 5:3632. [PubMed: 24709694]
14. a) Fan DL, Zhu FQ, Cammarata RC, Chien CL. Nano Today. 2011; 6:339–354.b) Fan D, Zhu F, Cammarata R, Chien C. Phys Rev Lett. 2005:94.c) Fan DL, Zhu FQ, Cammarata RC, Chien CL. Appl Phys Lett. 2004; 85:4175–4177.
15. a) Campion A, Kambhampati P. Chem Soc Rev. 1998; 27:241.b) Xu XB, Kim K, Li HF, Fan DL. Adv Mater. 2012; 24:5457–5463. [PubMed: 22887635] c) Xu X, Li H, Hasan D, Ruoff RS, Wang AX, Fan DL. Adv Funct Mater. 2013; 23:4332–4338.
16. a) Klipp, E.; Liebermeister, W.; Wierling, C.; Kowald, A.; Lehrach, H.; Herwig, R. Systems Biology. Wiley-Blackwell; 2009. b) Arlett JL, Myers EB, Roukes ML. Nature Nanotech. 2011; 6:203–215.
17. Férey G. Chem Soc Rev. 2008; 37:191. [PubMed: 18197340]
18. a) Lee KJ, Nallathamby PD, Browning LM, Osgood CJ, Xu XHN. ACS Nano. 2007; 1:133–143. [PubMed: 19122772] b) Greulich C, Kittler S, Epple M, Köller M. 2009; 38:11–13.c) Samberg ME, Loboa EG, Oldenburg SJ, Monteiro-Riviere NA. Nanomedicine-Uk. 2012; 7:1197–1209.d) Lin J-J, Lin W-C, Li S-D, Lin C-Y, Hsu S-h. Acs Appl Mater Inter. 2013; 5:433–443.e) Pauksch L, Hartmann S, Rohnke M, Szalay G, Alt V, Schnettler R, Lips KS. Acta Biomaterialia. 2014; 10:439–449. [PubMed: 24095782]
19. Amendola V, Bakr OM, Stellacci F. Plasmonics. 2010; 5:85–97.
20. Whitney TM, Searson PC, Jiang JS, Chien CL. Science. 1993; 261:1316–1319. [PubMed: 17731862]
21. a) Yi DK, Selvan ST, Lee SS, Papaefthymiou GC, Kundaliya D, Ying JY. J Am Chem Soc. 2005; 127:4990–4991. [PubMed: 15810812] b) Graf C, Vossen DLJ, Imhof A, van Blaaderen A. Langmuir. 2003; 19:6693–6700.
22. Willets KA, Van Duyne RP. Annu Rev Phys Chem. 2007; 58:267–297. [PubMed: 17067281]

23. a) Hu M, Ou FS, Wu W, Naumov I, Li X, Bratkovsky AM, Williams RS, Li Z. J Am Chem Soc. 2010; 132:12820–12822. [PubMed: 20795668] b) Schmidt MS, Hübner J, Boisen A. Adv Mater. 2012; 24:OP11–OP18. [PubMed: 22105972]
24. a) Le Ru EC, Etchegoin PG. Annu Rev Phys Chem. 2012; 63:65–87. [PubMed: 22224704] b) Blackie EJ, Le Ru EC, Etchegoin PG. J Am Chem Soc. 2009; 131:14466–14472. [PubMed: 19807188]
25. Le Ru EC, Blackie E, Meyer M, Etchegoin PG. J Phys Chem C. 2007; 111:13794–13803.
26. Fan DL, Cammarata RC, Chien CL. Appl Phys Lett. 2008; 92:093115.
27. a) Fan DL, Zhu FQ, Xu X, Cammarata RC, Chien CL. Proceedings of the National Academy of Sciences. 2012; 109:9309–9313.B) Jones, TB. Electromechanics of Particles. Cambridge University Press; New York: 1995.
28. Brad, AJ.; Faulkner, LR. Electrochemical Methods. Wiley; New York: 1980.
29. Munson, BR.; Young, DF.; Okiishi, TH. Fundamentals of Fluid Mechanics. 4. John Wiley; 2002.
30. a) Nikolic J, Expósito E, Iniesta J, González-Garcia J, Montiel V. J Chem Educ. 2000; 77:1191.b) Levich, VG. Physicochemical Hydrodynamics. Prentice-Hall; New York: 1962.

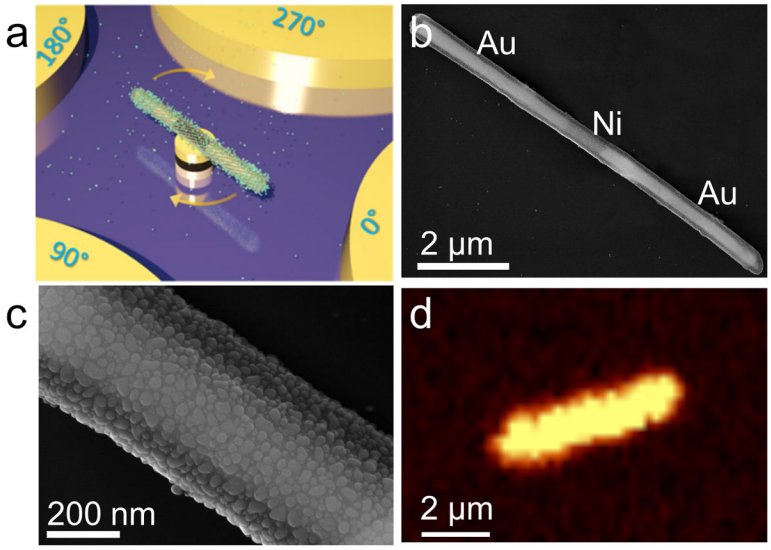

Figure 1.

(a) Schematic diagram of a rotating nanomotor sensor releasing molecules. (b) Scanning electron microscopy (SEM) images of a plasmonic nanorod for the nanomotor rotor made of a three layer structure with a Au-Ni-Au nanowire as the core, a silica coating, and a dense layer of Ag nanoparticles on the outer surface of silica, (c) a higher magnification SEM image shows the dense Ag nanoparticles grown on the silica. (d) Raman mapping of 1 μM R6G dispersed on a plasmonic nanomotor rotor showing essentially uniform SERS intensity on the surface.

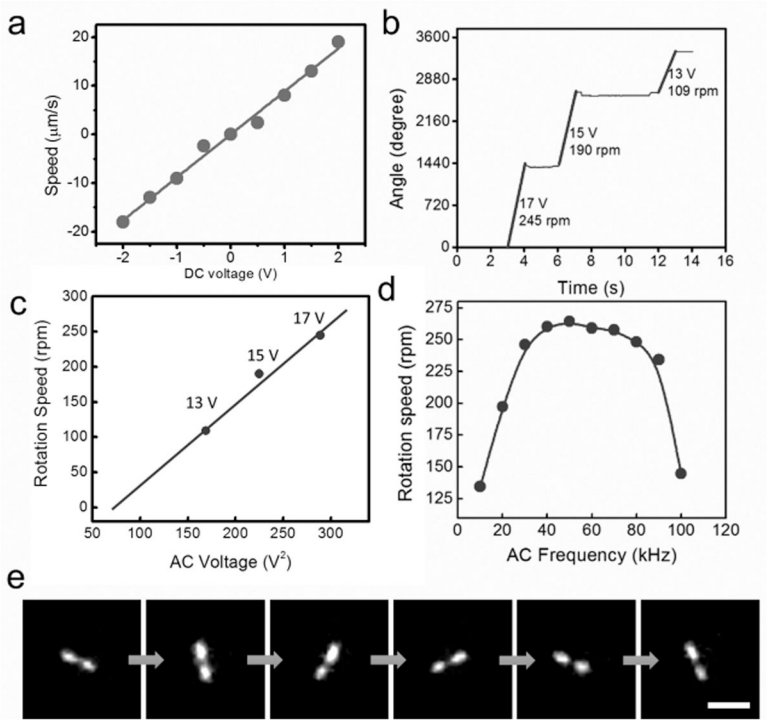

Figure 2.

(a) The transport speed of the plasmonic nanorotor increases with the applied DC voltages. (b, c) The rotation speed of nanomotor sensors increases linearly with V^2 (20 kHz), (d) and depends on the applied AC frequency (15 V). (e) Snapshots (every 1/6 second) of a rotating nanomotor functionalized with NB imaged in the Raman mode. Note that the objective of the inverted microscope is underneath the rotating nanomotor. Thus the Raman image of the middle of the plasmonic nanomotor was blocked by the magnetic bearing. (Scale bar: 10 μm)

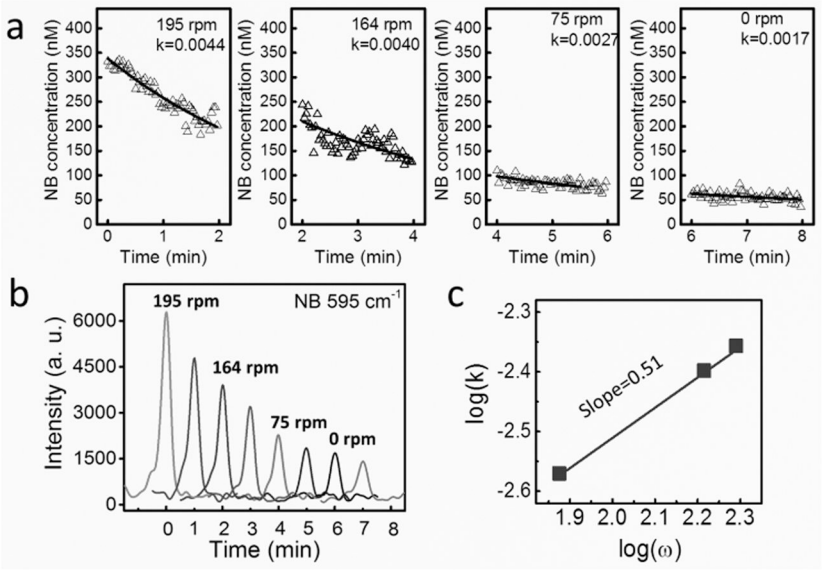

Figure 3.

Tunable release of biochemical by the mechanical rotation of nanomotor sensors. (a) Concentration of NB versus time at different rotation speeds. (b) Representative Raman spectra of R6G every 1 min at each rotation speed. (c) The release rate monotonically increases with the rotation speed with a power-law dependence of 0.51

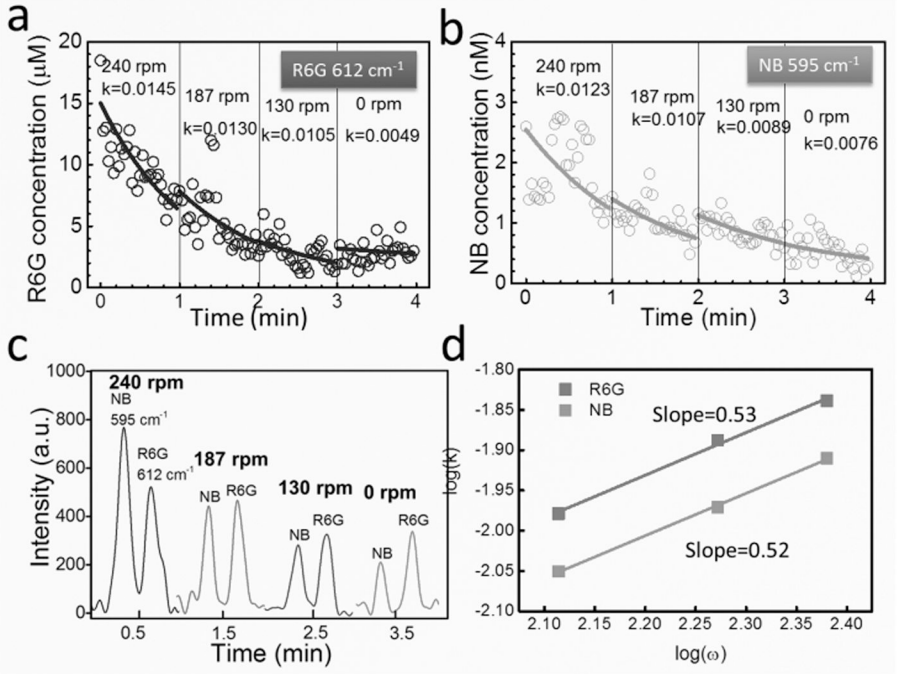

Figure 4.

Tunable release of bi-analytes [NB (a) and R6G(b)] functionalized on the same nanomotor by the rotation speed. (c) Representative Raman spectra of NB and R6G every 1 min at each rotation speed. (d) The release rates of both analytes of NB and R6G monotonically increase with the rotation speed with a power-law dependence of 0.52 and 0.53, respectively.

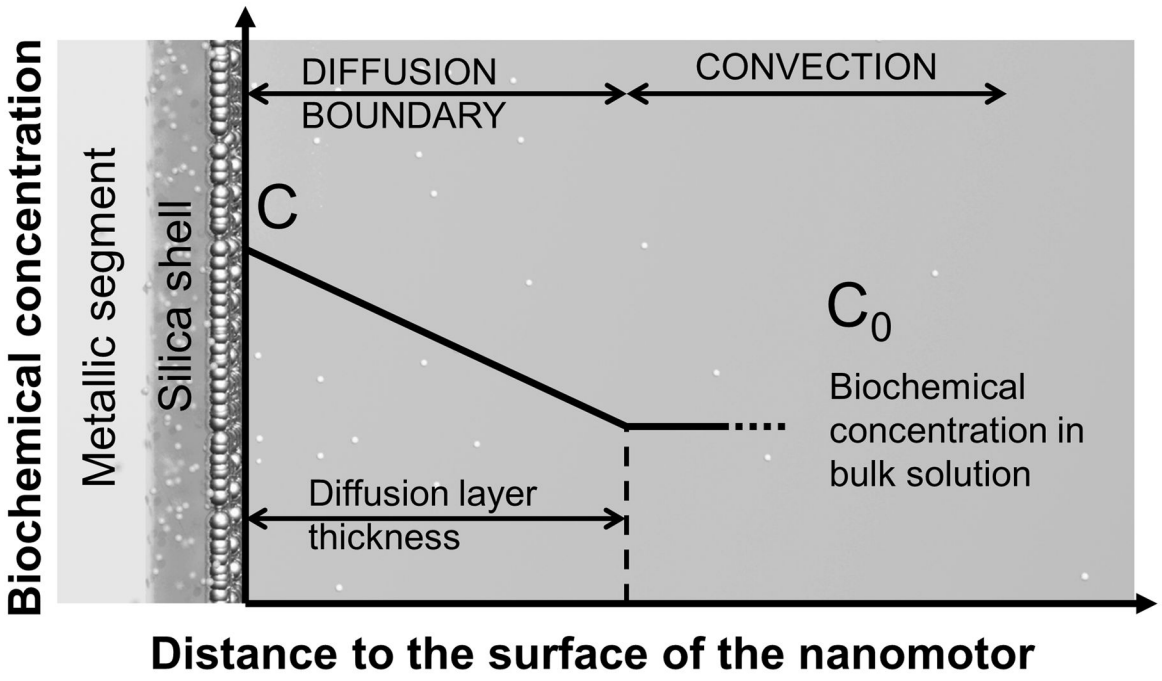

Figure 5.
Schematic diagram of the model of the diffusion boundary layer next to the surface of the nanomotor sensors. (small spheres: biochemical molecules; big spheres: Ag NPs)